Differential effect of 2-hydroxyoleic acid enantiomers on protein (sphingomyelin synthase) and lipid (membrane) targets ☆

Stefano Piotto [a,*], Simona Concilio [b], Erminia Bianchino [a], Pio Iannelli [a], David J. López [c], Silvia Terés [c], Maitane Ibarguren [c], Gwendolyn Barceló-Coblijn [c], Maria Laura Martin [c], Francisca Guardiola-Serrano [c], María Alonso-Sande [c], Sérgio S. Funari [d], Xavier Busquets [c], Pablo V. Escribá [c]

[a] Department of Pharmacy, University of Salerno, via Giovanni Paolo II 132, Fisciano 84084, SA, Italy
[b] Department of Industrial Engineering, University of Salerno, via Giovanni Paolo II 132, Fisciano 84084, SA, Italy
[c] Laboratory of Molecular Cell Biomedicine, University of the Balearic Islands — Lipopharma Therapeutics, S.L., Palma, Spain
[d] HASYLAB at Deutsches Elektronen-Synchrotron, D-22607 Hamburg, Germany

ARTICLE INFO

ABSTRACT

The complex dual mechanism of action of 2-hydroxyoleic acid (2OHOA), a potent anti-tumor compound used in membrane lipid therapy (MLT), has yet to be fully elucidated. It has been demonstrated that 2OHOA increases the sphingomyelin (SM) cell content via SM synthase (SGMS) activation. Its presence in membranes provokes changes in the membrane lipid structure that induce the translocation of PKC to the membrane and the subsequent overexpression of CDK inhibitor proteins (e.g., p21^{Cip1}). In addition, 2OHOA also induces the translocation of Ras to the cytoplasm, provoking the silencing of MAPK and its related pathways. These two differential modes of action are triggered by the interactions of 2OHOA with either lipids or proteins. To investigate the molecular basis of the different interactions of 2OHOA with membrane lipids and proteins, we synthesized the R and S enantiomers of this compound. A molecular dynamics study indicated that both enantiomers interact similarly with lipid bilayers, which was further confirmed by X-ray diffraction studies. By contrast, only the S enantiomer was able to activate SMS in human glioma U118 cells. Moreover, the anti-tumor efficacy of the S enantiomer was greater than that of the R enantiomer, as the former can act through both MLT mechanisms. The present study provides additional information on this novel therapeutic approach and on the magnitude of the therapeutic effects of type-1 and type-2 MLT approaches. This article is part of a Special Issue entitled: Membrane Structure and Function: Relevance in the Cell's Physiology, Pathology and Therapy.

© 2014 Elsevier B.V. All rights reserved.

1. Introduction

Membrane lipids not only fulfill an essential role in defining the cell barrier, but also play central roles in several cellular processes. Lipids influence the activity of membrane proteins by means of their chemical nature and the physical properties of lipid mixtures in function of their composition [1]. Eukaryotic cells contain a wide variety of membrane lipids, the proportions and types of which define different types of membrane microdomains, regions that regulate: (i) the activity of the proteins; (ii) their localization; and (iii) protein–protein interactions and ensuing signal propagation [2]. Moreover, lipid alterations are often associated with distinct conditions or pathological states, which in principal could be reversed by regulating the membrane lipid composition [3]. Indeed, therapeutic approaches aimed at regulating the lipid composition of the cell membrane have arisen as a relevant alternative to conventional chemotherapy. In this context, the two main mechanisms of membrane lipid therapy (MLT) identified are associated with the direct presence of the hydrophobic drug in the membrane (type-1 MLT) or the binding of the lipid to a protein (e.g., enzyme, flippase, and translocase) that regulates the membrane lipid composition, and that may modify lipid microdomains and cell signaling (type-2 MLT). Lipids are not covalently bound in membranes but rather, they are dynamically aggregated in transient structures with lateral and cross-sectional asymmetry. By contrast, amino acids occupy defined positions in protein binding sites and for this reason, the structural features that determine the interaction of ligands with proteins and lipids show important divergence. In the present study, we compared the interaction of 2OHOA (Minerval), its enantiomers and related fatty acid analogs, with proteins and lipids. We show here the important differences in the interaction of the R and S enantiomers of Minerval (RMI and SMI, respectively) with one of its targets, SGMS, but not with the other target known, the lipid bilayer. Interestingly, despite the differences in molecular interactions and signal regulation, the result of both type-1 MLT and type-2 MLT merges to produce anti-tumor effects whose potency can be ascribed semi-quantitatively to either

mechanism of action. 2OHOA already attracted the interest of computational scientists who investigated the effect of 2OHOA on model membranes [4,5]. Cerezo and coworkers observed that the hydroxyl group of 2OHOA induces a displacement of the FA chains along the bilayer normal towards the outer side of the membrane. This could be associated with a better packing of the headgroup area, which would account in turn for the observed shift of the Lα-to-H$_{II}$ phase transition at high temperatures and for the subsequent stabilization of the Lα phase. Up to now, no information is available on the different behaviors of the R and S isoforms of 2OHOA in model membranes differing in fluidity.

We have investigated the effect of natural and synthetic fatty acids (FAs) on the structure of the lipid bilayer by molecular dynamics. We used model membranes formed by 1-palmitoyl, 2-oleoyl-sn-glycero-3-phosphocholine (POPC) and POPC:1-palmitoyl-2-oleoyl-sn-glycero-3-phosphoethanolamine (POPE) as liquid-disordered (L$_d$) membrane model, and sphingomyelin:cholesterol (SM:CHO) as models of liquid-ordered (L$_o$), raft-like microdomains. The similar interaction of 2OHOA enantiomers with these membranes was demonstrated by molecular dynamics and confirmed by X-ray diffraction. Likewise, their interaction with SGMS and its ensuing activation was determined through the production of SM in U118 cells [6,7]. Finally, the therapeutic efficacy of 2OHOA, and its R and S enantiomers was evaluated in an animal model of human lung cancer, in which it could be determined that type-1 and type-2 mechanisms may account for about one and two thirds of the therapeutic effects triggered by this compound, respectively. This study provides relevant information about the molecular bases of the pharmacological mechanisms of 2OHOA, and it highlights the important differences between the direct action of this compound on the structure of the lipid bilayer and on the activity of the SGMS enzyme.

2. Materials and methods

2.1. Materials

POPE was purchased from Avanti Polar Lipids (Alabaster, AL, USA). NaCl, HEPES and EDTA were obtained from Scharlau (Barcelona, Spain). RMI and SMI were provided by Lipopharma Therapeutics S.L. (Palma de Mallorca, Spain), while the racemic (R + S) mixture of 2OHOA (2OHOA) was prepared by mixing equimolar amounts of both enantiomers. Lipid standards for thin layer chromatography assays were from Larodan Fine Chemicals (Malmö, Sweden). 2,3-bis[2-Methoxy-4-nitro-5-sulfophenyl]-2H-tetrazolium-5-caboxyanilide inner salt (XTT), heparin sodium salt, RPMI-1640 and Dulbecco's Modified Eagle's Medium were purchased to Sigma-Aldrich (Madrid, Spain). The bicinchoninic protein quantification kit was obtained from Thermo Scientific (Waltham, MA) and silica gel 60 plates (20 × 20 cm, 250 μm) were from Whatman (Kent, United Kingdom).

2.2. Molecular dynamics

2.2.1. Construction of computational molecular models of lipid membranes

Four model membranes have been built, one of which was made of POPC and a second membrane in which POPC was mixed with POPE at a molar ratio of 1:1. The coordinates of both membranes were taken from a previous work [8]. Two other membranes were made of different molar ratios of SM and CHO, 6:4 and 8:2. All lipids forming a membrane were automatically preassembled, solvated in TIP3P water with 150 mM NaCl and subsequently allowed to relax to experimental values in terms of area per lipid and bilayer thickness. In order to study the interaction of oleic (OA), elaidic (EA), stearic (SA) acids and the two enantiomers of 2OHOA (RMI and SMI) with the SM:CHO model membranes, we replaced one lipid molecule in each layer with two molecules of OA, EA, SA, RMI or SMI (see Fig. 1). Two FA molecules were used because their volume, ranging from 300 Å^3 to 306 Å^3, for EA and 2OHOA molecules, respectively, is similar to that of SM or POPC. The lipid bilayers were relaxed by reducing the box dimension until the van

der Waals energy of the system started to increase [8,9], and the structural parameters of the membranes generated were similar to those measured in model membranes [10]. To avoid abnormal atom–atom collisions and to correct the covalent geometry, the energy of all the systems was minimized. After the removal of conformational stress by a short steepest descent minimization, the procedure was continued by simulated annealing (time step 2 fs, atom velocities scaled down by 0.9 every 10 steps) until convergence was reached, i.e. the energy improved by less than 0.05 kJ/mol per atom during 200 steps. A full description of the protocols is given in [8]. The position of FAs inside membranes was determined by means of 120 replicas of each membrane/FA system in which the FA molecules were placed and relaxed in different positions through the bilayer. Short dynamics of 1 ns and subsequent minimizations have been performed to calculate the approximate free energy of binding. The replicas having the energy minimum were chosen as initial structure for the production run. The lipid composition and physical parameters of the L$_o$ and L$_d$ model membranes used are shown in Table 1.

2.2.2. Molecular dynamics simulation

All the simulations were performed with the YASARA program [11] under a NPT ensemble at 310 K and 1 atm, coupling the system to a Berendsen thermostat and barostat [12] coupled to a water density control as implemented in this software. The AMBER03 force field was used [13], and the geometry of the molecules was optimized with a semi-empirical AM1 method using the COSMO solvation model [14]. Partial atomic charges were calculated using the same level used in the Mulliken point charge approach [15]. Electrostatic interactions were calculated with a cutoff of 10.48 Å, and the long-range electrostatic interactions were handled by the Particle Mesh Ewald [16] algorithm, using a sixth-order B-spline interpolation and a grid spacing of 1 Å. The leap-frog algorithm was used in all the simulations, with a 1.25 fs time step for intramolecular forces, and 2.5 fs time step for intermolecular forces. The production runs were of 50 ns and the trajectories were recorded every 5 ps. Though this time is short to observe the spontaneous insertion of the FAs, it is a convenient time to derive important structural data of the membrane at equilibrium.

2.2.3. Theory/calculation

2.2.3.1. Energies and structural parameters.
Energies and structural parameters were calculated following standard procedures and equations. Here we focused on the stabilization/destabilization of the membrane upon addition of an exogenous FA calculating the intramolecular energy of the membrane lipids. The solvation free energy of the membrane does not change significantly upon addition of FAs and it is not reported here.

The calculation of the potential energy was accurate enough to calculate relative stability of the different systems. The potential energy per lipid was calculated by dividing the total potential energy of the membrane by the number of lipids. The thickness was determined as the average distance between the planes fitting the phosphorous atoms of the two layers. The polarization of water dipoles on the bilayer surface (expressed in Debye) was calculated by averaging the dipole moment of water molecules with a distance <4 Å from the membranes. For comparison, the average dipole moment of water in bulk is <0.037 D. The error is calculated by averaging 5 snapshots of the last 5 ns of simulations. The calculation of membrane properties in function of the depth in the bilayer was performed by dividing the membrane into rectangular slabs of 1 Å thickness and lying perpendicular to the z axis (normal to the bilayer). This procedure was adopted to calculate the profiles of mass density and lateral pressure profile as a function of z.

2.2.3.2. Mass density profiles.
The cross-sectional mass distribution analysis of the lipid bilayer provides valuable information about the

Table 1
Composition and physical characteristics of the different model membranes studied by molecular dynamics.

Membrane structure	Lipid composition (mol ratio)	Number of lipid molecules	Number of ions and water molecules (Cl^-:Na^+:H_2O)	Simulation box average dimensions (Å) (X;Y;Z)
Lo	SM:CHO (6:4)	146:99	26:26:9264	68.69;70.17;106.25
	SM:CHO (8:2)	175:44	21:24:8609	67.31;68.22;106.57
	SM:CHO:FA (6:4)	144:99:4	24:26:9287	68.56;69.54;104.28
	SM:CHO:FA (8:2)	173:44:4	21:24:8609	67.31;68.22;106.57
Ld	POPC:POPE (10:0)	98:0	24:24:8265	57.18;56.42;120
	POPC:POPE (6:4)	58:40	20:20:7098	56.69;53.79;109.4
	POPC:POPE:FA (10:0)	96:0:4	24:24:8265	57.18;56.42;120
	POPC:POPE:FA (6:4)	56:40:4	20:20:7098	56.69;53.79;109.04

structural changes in membranes. For lipids, the mass density profile indicates the atom distribution along the bilayer. These profiles are determined by dividing the simulation box into a number of thin slices of equal thickness along the normal direction of the bilayer, and by finding the mass density of the atoms located in each slice and by time averaging over a large number of snapshots evenly distributed over the simulation time interval (i.e.: the last 25 ns of the 50 ns simulation). This approach can be used because the membranes remain approximately flat throughout the simulation period.

2.2.3.3. Lateral pressure profile. The mechanical properties of a membrane can be described by all the forces acting in the plane of the bilayer. At equilibrium, the bilayer adjusts the area per lipid so that the sum of these forces or lateral pressures is zero. However, they may vary in function of the depth of the bilayer, as expressed by the lateral pressure or stress profile across the bilayer, p(z). Changes in the membrane lipid composition modify the shape of the lateral pressure profile, which in turn alters the amount of mechanical work associated with conformational changes in membrane proteins [17]. Using molecular dynamics to compare the pressure profile of model membranes with those of membranes modified by FAs provides valuable data, because such effects cannot be measured experimentally [18]. The lateral pressure profile was calculated using the method described by Hardy [19], evaluating the stress of membrane slices perpendicular to the z axis.

2.2.3.4. Radial distribution function. The radial distribution function (RDF) describes how the mass density varies as a function of the distance from a reference atom. The RDF of atoms relative to each other (i.e. N-N RDF) is given by:

$$RDF = \frac{V}{N}\left\langle \frac{n(r)}{4\pi r^2 dr} \right\rangle,$$

where n(r) is the number of atoms in the spherical ring of radius r and width dr around the given atom, $4\pi r^2 dr$ is the volume of the ring; and < > denotes the time and ensemble average.

2.2.3.5. CHO charge distribution. To verify if the presence of 2OHOA and other FAs could induce a change in the charge distribution on CHO, we calculated the atom charges in different environments: CHO in water, CHO embedded in an equilibrated SM:CHO membrane, and finally, CHO embedded in an equilibrated SM:CHO membrane (6:4, mol:mol) after the addition of 2OHOA. The computational method aimed to study portions of membranes that usually deal with chemical models too large to be handled by ab initio methods. However, the full quantum mechanical treatment of a large molecular model is possible when using semi-empirical methods in combination with linear scaling techniques. We have optimized the membranes using the MOZYME LMO [20] method. Subsequent single point energy calculations were performed using the PM6 method [21] without using MOZYME. This is required to avoid accumulating MOZYME energy errors during geometric optimization.

2.3. X ray diffraction

In all cases, lipids were initially stored at −20 °C in chloroform:methanol (2:1; v:v). POPE was combined with 5 mol% of RMI, SMI or the racemic mixture of 2OHOA, the solvent was first evaporated under argon flow and the remaining solvent traces were removed under vacuum for 12 h. The lipid film (15% w:w) was then resuspended in 10 mM HEPES, 100 mM NaCl, 1 mM EDTA, pH 7.4, following 5 freeze–thaw cycles, with gentle vortexing between cycles to favor resuspension. Samples were left at 4 °C for 24 h before use.

Small- and wide-angle (SAXS and WAXS) synchrotron radiation X-ray scattering data was collected simultaneously, using standard procedures on the Soft Condensed Matter Beamline A2 of the Hasylab at the DORIS III storage ring of the Deutsches Elektronen Synchrotron, Hamburg. Samples were loaded into 1 mm borosilicate capillaries, flame-sealed and stored at 4 °C. Data were acquired using a local shutter to irradiate the sample using the following sequence: 10 s opened–3 s closed–10 s opened–32 s closed. During data collection, the samples were heated from 20 °C to 80 °C at a scan rate of 1 °C/min, and the samples were maintained at the highest temperature for 5 min before they were finally cooled to 15 °C at the same scan rate. The SAXS data were analyzed at all temperatures, while the WAXS signals were only collected between 15 °C and 25 °C in order to detect gel structures. The experimental conditions did not affect the phase sequence structures or their parameters. The positions of the observed peaks were converted into distances (d) after calibration with the rat tendon tail and poly-(ethylene terephthalate) standards for SAXS and WAXS regions, respectively.

Interplanar distances, d_{hkl}, were calculated according to equation

$$S = \frac{1}{d_{hkl}} = \frac{(2\sin\theta)}{\lambda}$$

where S is the scattering vector, 2θ is the scattering angle, λ (0.154 nm) is the X-ray wavelength and hkls are the Miller indexes of the scattering planes.

2.4. Cell culture

All cell lines were grown at 37 °C in an atmosphere of 5% CO_2/80–95% relative humidity. Human glioma (U118) and non-small cell lung cancer (A549) cells were obtained from the European Collection of Cell Cultures. They were cultured in 2 mM glutamine-supplemented RPMI 1640 medium, containing 5% fetal bovine serum (by vol.), 100 units/ml penicillin, and 100 μg/ml streptomycin. MRC5 human fibroblasts, from the American Type Culture Collection, were cultured in Dulbecco's Modified Eagle's Medium supplemented with 1% non-essential amino acids (by vol.), 10% fetal bovine serum (by vol.), 100 units/ml penicillin and 100 μg/ml streptomycin.

2.5. Determination of SM levels after 2OHOA treatment

When U118 cells reached 50% confluence, they were exposed to 100 μM of RMI, SMI or RMI:SMI (1:1; w:w) mixture for 24 h, after

which the total cell lipids were extracted directly from the frozen cell monolayers as described elsewhere [22]. Briefly, cells were scrapped and for each 1 ml of sample, 3.75 ml of chloroform:methanol (1:2, v/v) was added and thoroughly agitated in a vortex for 1 min. Subsequently, 1.25 ml of chloroform was added and the mixture was again vortexed thoroughly for 1 min. Finally, 1.25 ml of 1 M NaCl was added and mixed thoroughly in a vortex for 30 s. The samples were then centrifuged at 1000 g for 5 min at room temperature, and the lower organic phase was recovered and stored in an atmosphere of N_2 at -80 °C. In order to measure the protein content, 10 µl aliquots were taken from the samples before extraction and they were stored at -20 °C. The protein was measured using the bicinchoninic assay according to the manufacturer's instructions. Individual phospholipid classes were separated by thin layer chromatography on Whatman silica gel 60 plates (20 × 20 cm, 250 µm), previously heat-activated at 110 °C for 1 h. Phospholipids were separated using chloroform:methanol:acetic acid:water (55:37.5:3:2, by volume), and the plates were air-dried after development, sprayed with 8% H_3PO_4 (w/v) containing 10% $CuSO_4$ (w/v), and charred at 180 °C for 10 min [23]. The lipids were identified using commercially available standards and they were quantified using a GS-800 densitometer from Bio-Rad (Hercules, CA). The concentration of the SGMS product, SM, was determined in at least 4 independent experiments performed in triplicate.

2.6. Cell proliferation assay

MRC5 and A549 cells were cultured as indicated above and their proliferation was determined using the XTT method. Briefly, cells were seeded in 96-well plates at a density of 2.5–5×10^3 cells per well 12–24 h before treatment. Then, cells were incubated for different times with 0–2000 µM racemic 2OHOA or its enantiomers, following 2 h at 37 °C in medium containing XTT, according to the manufacturer's instructions. The cell viability was calculated measuring the absorbance at 450 nm on a FLUOstar Omega microplate reader from (BMG Labtech; Ortenberg, Germany). To determine the correspondence between the absorbance and the number of viable cells, duplicate plates cultured in parallel under the same conditions but at increasing cell densities were counted using the trypan blue exclusion method.

2.7. Tumor growth and animal treatments

For in vivo studies, A549 human lung cancer cells were cultured under the above described conditions and 7.5×10^6 cells in a total volume of 200 µl were inoculated subcutaneously into the dorsal area of male NUDE (Swiss) Crl:NU(Ico)-Foxn1^{nu} mice (5 weeks old, 30–35 g: Charles River Laboratories, Paris, France). After one week, when tumors were already visible, animals were randomly divided into groups and they were orally administered the vehicle (water), 2OHOA, RMI or SMI (400 mg/kg, daily, p.o.). After 21 days of treatment, the tumor volumes were calculated by

$$V = W^2 \times L/2$$

where V is the volume of the tumor, W is the tumor width and L, its length. The data obtained are expressed as the mean ± s.e.m. of the values from 12 animals. The differences between experimental groups were considered statistically significant at $P < 0.05$: $^*P < 0.05$, $^{**}P < 0.01$, and $^{***}P < 0.001$.

3. Results

3.1. Energy and density profiles

The values of the potential energy per lipid molecule (Table 2) indicate that the FAs studied can insert easily into POPC and POPC:POPE membranes. The insertion of RMI and SMI was thermodynamically more favorable into Ld than Lo membranes. Both RMI and SMI slightly increased the thickness of non-raft bilayers, while all the other FAs did not alter the cross-sectional membrane organization. Concerning the lipid raft-like bilayers, both 2OHOA enantiomers induced a slight thinning of SM:CHO 6:4 (mol:mol) bilayers. After the addition of different FAs, mass density profiles of POPC:POPE (6:4; mol:mol) (Fig. 2A) or SM:CHO (6:4; mol:mol) (Fig. 2B) membranes showed that the insertion of RMI or SMI increased the penetration of water molecules towards the lipid bilayer core.

Table 2
Summary of the simulations of preassembled bilayer systems.

| Membrane composition	FA	Energy per lipid (kcal/mol)	Thickness (Å)	Water polarization (Debye)
POPC	None	-242.31 ± 0.52	35.30 ± 0.44	0.22 ± 0.04
	EA	-247.02 ± 0.63	34.92 ± 0.35	0.43 ± 0.03
	OA	-269.32 ± 0.54	35.94 ± 0.42	0.32 ± 0.05
	SA	-246.97 ± 0.72	35.06 ± 0.33	0.41 ± 0.04
	RMI	-246.22 ± 0.69	35.22 ± 0.34	0.44 ± 0.05
	SMI	-245.82 ± 0.69	35.26 ± 0.34	0.44 ± 0.05
POPE:POPC (6:4)	None	-208.82 ± 0.43	37.00 ± 0.28	0.41 ± 0.05
	EA	-210.80 ± 0.63	37.34 ± 0.34	0.34 ± 0.04
	OE	-210.78 ± 0.53	36.35 ± 0.34	0.34 ± 0.03
	SA	-210.20 ± 0.65	37.72 ± 0.33	0.40 ± 0.03
	RMI	-210.76 ± 0.53	38.56 ± 0.30	0.42 ± 0.04
	SMI	-210.32 ± 0.53	38.50 ± 0.30	0.43 ± 0.04
SM:CHO (8:2)	None	-123.73 ± 0.52	49.06 ± 0.29	0.59 ± 0.06
	EA	-124.30 ± 0.47	49.67 ± 0.34	0.47 ± 0.05
	OA	-124.46 ± 0.64	49.36 ± 0.33	0.57 ± 0.05
	SA	-125.28 ± 0.63	48.87 ± 0.36	0.53 ± 0.06
	RMI	-123.08 ± 0.55	49.02 ± 0.40	0.48 ± 0.05
	SMI	-123.02 ± 0.54	49.22 ± 0.40	0.45 ± 0.04
SM:CHO (6:4)	None	-115.98 ± 0.57	49.11 ± 0.34	0.41 ± 0.04
	EA	-115.85 ± 0.38	48.69 ± 0.24	0.41 ± 0.03
	OA	-116.22 ± 0.54	48.58 ± 0.26	0.36 ± 0.04
	SA	-116.26 ± 0.83	48.98 ± 0.28	0.37 ± 0.04
	RMI	-115.77 ± 0.53	48.05 ± 0.39	0.37 ± 0.04
	SMI	-115.88 ± 0.52	48.09 ± 0.36	0.37 ± 0.04
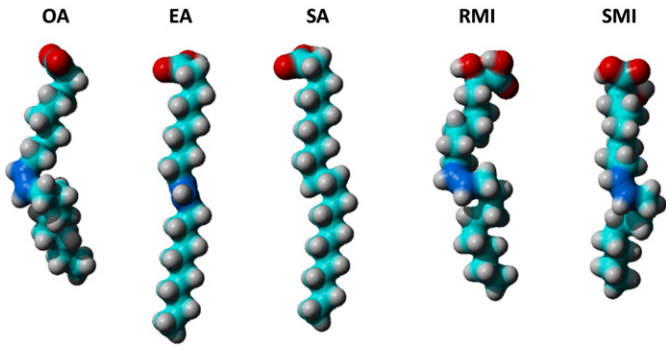
Fig. 1. Atom representation of the FAs used in the simulations (in red, oxygen: cyan, sp³ carbon; gray, hydrogen; blue, sp² carbon).
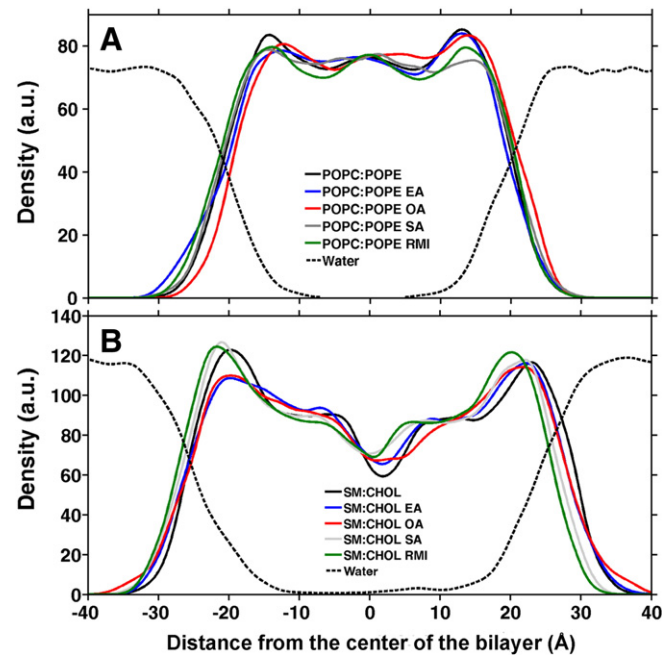

Fig. 2. Mass density profiles: (A) comparison between the global density of POPC:POPE membranes in the presence or absence of different FAs. (B) SM:CHO 6:4 (mol:mol) membrane in the presence or absence of different FAs. Control membranes are shown in black, EA in blue, OA in red, SA in gray and RMI in green. The density of water molecules is shown as a continuous line. SMI is not shown because it overlaps with RMI.
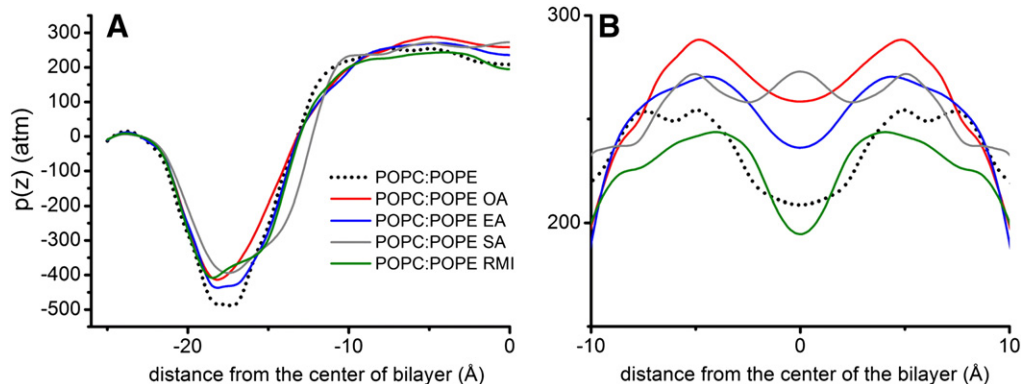
3.2. Lateral pressure profiles

We examined the effect of FAs on the lateral pressure profile p(z) (Figs. 3 and 4). Positive values of p(z) correspond to pressures that tend to expand the membrane, while negative values correspond to a tendency to compress it. Thus, for each leaflet of the bilayer there is a negative peak contributed by the balance between the solvent-headgroup interface and the headgroup–tailgroup interface, both negative, while the bilayer headgroup region has a positive pressure value. The fatty acyl region of the bilayer has a positive pressure value due to the packing of the tails, with mild tension in the middle of the bilayer at the ends of the lipid tails.

The profiles in POPC:POPE membranes containing different free FAs were assessed (Fig. 3). All these bilayers have zero net tension ($\gamma = 0$), such that the area under of the p(z) curves integrates to zero. Although the shape of p(z) remains similar, the FAs reduce the magnitudes of the negative peaks. The strongest reduction was observed with 2OHOA, with no significant differences between RMI and SMI, and this reduction in the negative peak suggests an increased propensity for water penetration. Both forms of 2OHOA also have a very modest effect on the lateral stress in the membrane core, whereas all the other FAs induce a mild increase in positive pressure. Similar trends were observed in POPC membranes.

Interestingly, FAs have a marked effect on the lateral packing of SM and CHO molecules in raft-like membranes, with pressure changes of more than 150 atm (Fig. 4). Indeed, the longest FA of the series, EA, induces an increase of ca. 250 atm at the center of the bilayer. By contrast, SA and more clearly, RMI and SMI, induce a mild relief of about 40 atm in pressure at the center of the membrane.

3.3. Water electric dipole orientation and charge distribution on cholesterol

As described above for other biophysical membrane properties, 2OHOA induced opposing effects on bilayer hydration (as determined by RDF analysis) in Lo (SM:CHO) and Ld membranes (POPC or POPC:POPE) (Fig. 5). In this context, the trans-unsaturated FA, EA did not affect the hydration of POPC:POPE membranes, whereas the presence of saturated SA in the bilayer caused a reduction in the number of water molecules around the lipid headgroups. This was probably due to a reduction in surface fluctuation that limits the surface exposed to water. By contrast, the cis-monounsaturated FAs OA, RMI and SMI increased the hydration of the membrane surface. In Lo membranes, all FAs increased water hydration. Above all, SA and EA with a linear geometry, as well as the two 2OHOA enantiomers, augment the density in the first shell of hydration. To quantify the increase in hydration, we integrated the RDF function between 2 and 3 nm, and we found that SA,
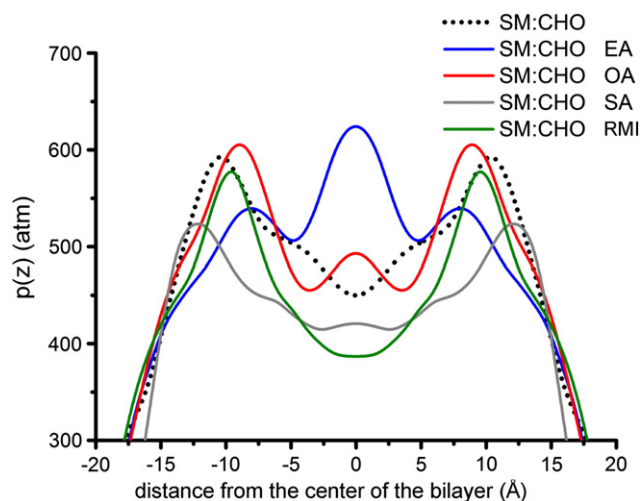

Fig. 3. Lateral stress profiles. Comparison of the POPC:POPE membranes after FA addition: the POPC:POPE membrane is shown with a dotted black line, EA in blue, OA in red, SA in gray, and RMI in green. (A) Close up of the negative peaks in the headgroup region. (B) Close up of the positive pressure region at the center of the bilayer. SMI is not shown because it overlaps with RMI.

Fig. 4. Lateral stress profiles. Comparison of the SM:CHO 6:4 (mol:mol) membranes after FA addition: the SM:CHO membrane is shown with a dotted black line, EA in blue, OA in red, SA in gray and RMI in green. (A) Close up of the negative peaks in the headgroup region. SMI is not shown because it overlaps with RMI.

EA and 2OHOA increased the surface hydration by about 15%. Moreover, we were unable to detect relevant differences between RMI and SMI with regards their influence on surface hydration (Fig. 5).

Additional information about the water ordering in the proximity of the membrane–solvent interface (hydration layer) can be obtained by studying the time-averaged projections of water electric dipole unit vectors onto the normal bilayer unit vector, $\mathbf{n}$. The polarization of water dipoles at the bilayer surface (reported in Table 2) indicated that EA and OA decreased the average dipole moment in more fluid membranes (POPC, POPC:POPE), whereas the effect of SA falls within the experimental error. By contrast, 2OHOA increased water polarization due to the presence of an additional hydroxyl group on the membrane surface. In raft-like membranes, all FAs, including the 2OHOA enantiomers, show a reduction of water polarization, an effect that would be the result of a decrease in the ordering of the membrane surface, but the reduction is comparable with the error and these data must be taken with caution. The changes at the membrane surface induced a reorganization of the membrane core, as shown above for lipid bilayer lateral pressure profiles. When the membrane core reorganizes, CHO may adopt a distinct charge distribution and its distortion, induced by the lipid environment, is reflected in the change in charge of the CHO head. However, CHO atoms distant from the bilayer surface showed no significant change (Fig. 6).
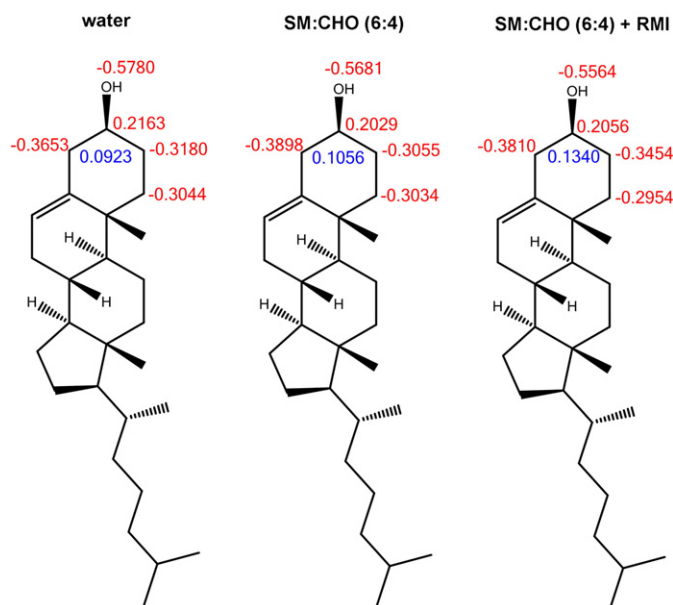

Fig. 6. Atom charges of CHO after geometry optimization with MOZYME and subsequent PM6 (MOPAC) calculation in water (upper figure), in SM:CHO membranes (center figure) and SM:CHO membranes containing RMI (lower figure). Only atoms that underwent to a charge changes larger than 5% are reported. In red is indicated the carbon or oxygen atoms; in blue is indicated the charge of hydrogens.

3.4. 2OHOA–membrane interactions by X-ray diffraction

Molecular dynamics experiments suggest that both 2OHOA enantiomers, as well as the racemic form, induce a similar effect on the membrane lipid structure. Here we used POPE membranes containing 5 mol% of either racemic 2OHOA or its R and S enantiomers to study the effects of the optical isomers of 2OHOA on the lipid bilayer structure. X-ray diffraction studies (Fig. 7) showed that either RMI, SMI or the racemic mixture of 2OHOA affected POPE structure in a similar manner. These data confirm the molecular modeling studies showing that the relative position of the carboxyl and hydroxyl groups in the 2OHOA molecule does not have an important impact on its interactions with phospholipids. In recent years, we have studied the interaction of different FAs with membranes and as such, more details on the effects of saturated (e.g., SA) and unsaturated (2OHOA, EA and OA) fatty acids on membrane lipid structure can be found elsewhere [24–26].
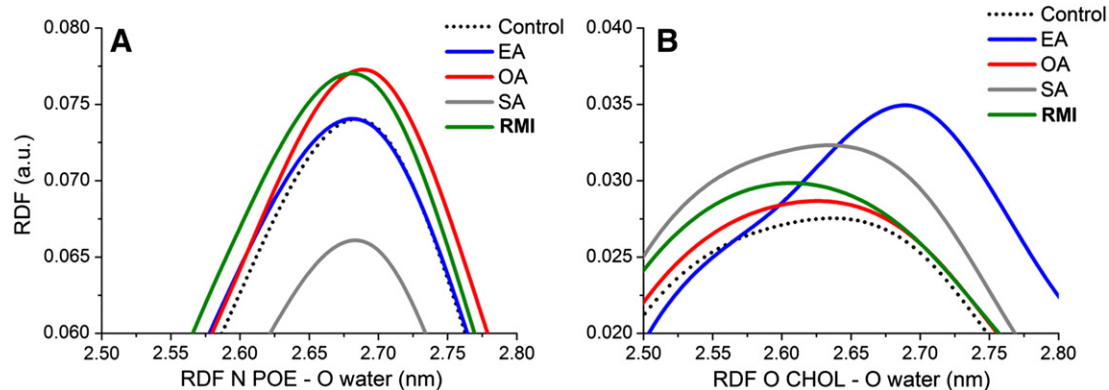

Fig. 5. Radial distribution functions. (A) RDF of the N atom of POPE with water oxygen atoms in POPC:POPE membranes. (B) RDF of the CHO oxygens with water oxygen atoms. SMI is not shown because it overlaps with RMI.
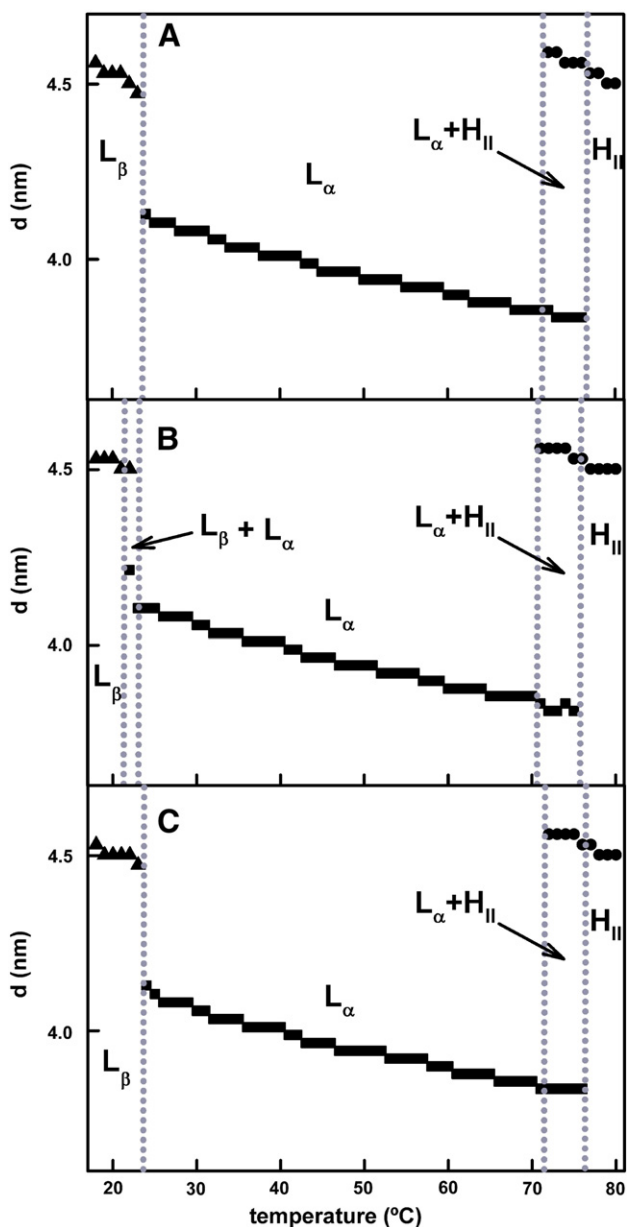
Fig. 7. Temperature dependence of the interplanar repeat distances (d) of vesicles composed of (A) POPE + 5 mol% RMI, (B) POPE + 5 mol% SMI and (C) 2OHOA (racemic mixture). Samples were loaded in a borosilicate capillary and heated to between 20 and 80 °C at a scan rate of 1 °C/min. Gel (L_β), fluid (L_α) and hexagonal (H_{II}) phases, as well as the coexistence of lipid phases are indicated in each graph using SAXS data. The presence of L_β was confirmed by WAXS measurements.

3.5. Effects of 2OHOA enantiomers on cellular levels of SM

We previously showed that 2OHOA activates SGMS, the enzyme that transforms PC and PE into SM [6,7]. Here, we show for the first time the effect of both 2OHOA enantiomers on levels of cellular SM (Fig. 8). Interestingly, the S enantiomer, but not the R isomer, was responsible for the transformation of PC and PE into SM in U118 human glioma cells. Meanwhile, the racemic mixture of 2OHOA elicited a similar behavior to that of SMI enantiomer.

The anti-tumor effect of 2OHOA is the result of a dual mode of action, in part due to the activation of SGMS [6,7] and also due to the presence of 2OHOA in membranes and the ensuing regulation of the membrane's lipid structure [6,24,25,27]. The first of these effects induces a large increase in SM, which augments the proportion and order of raft-like (L_o) membrane lipid domains as shown in lipid extracts from 2OHOA-
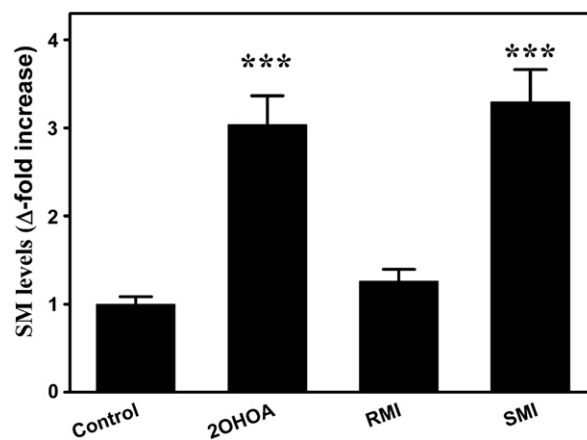

Fig. 8. Determination of SM levels upon treatment with 2OHOA. SM mass levels were determined in U118 cells exposed to 100 μM RMI, SMI or racemic 2OHOA for 24 h. SM content in treated cells was referred to control (untreated) cell values, which account for ca. 10% of total phospholipids (data taken from [6]). Lipids were separated by thin-layer chromatography and the amount of SM was determined by photodensitometry after spraying the plate with a solution of $CuSO_4$ (8%, w/v) and H_3PO_4 (10%, w/v) and charring it at 180 °C for 10 min. Values represent the mean ± s.e.m.; n = 8; *, $P < 0.05$; ***, $P < 0.001$.

treated cells (200 μM; 24, 48 and 72 h) reconstituted into liposomes [27]. 2OHOA treatment also induces Ras translocation to the cytoplasm and inactivation of the MAPK pathway [6,7]. Conversely, the presence of 2OHOA alone or bound to phospholipids reduces the ordering of L_d domains [6,27]. This second effect on lipid structure causes a mild (i.e.: 150–400%) and sustained (>24 h) activation of PKC that results in increased expression of CDK inhibitors, E2F1 inactivation and DHFR knockdown [25,28]. By contrast, with SGMS activation by the S enantiomer, both R and S enantiomers will produce similar effects on membrane structure and trigger this second mechanism of action.

3.6. Anti-cancer effects of 2OHOA enantiomers

Finally, we assessed the anti-tumor effect of 2OHOA and its enantiomers. We observed that the S enantiomer inhibited the growth of A549, lung adenocarcinoma cell line with an IC_{50} below that of the R form (184 μM and 252 μM, respectively). Interestingly, the racemic mixture exhibited similar values to those of SMI (181 μM). This result would be consistent with the combined effect of type-1 (direct binding to membranes) and type-2 (enzyme-mediated regulation of membrane lipid composition) MLT effects by SMI (and also that of the racemic form), whereas RMI would only act through a type-1 MLT mode of action. By contrast, 2OHOA and its enantiomers were not toxic against non-tumor MRC5 human fibroblasts at the concentration used against human lung adenocarcinoma cells. To further semi-quantify the anti-tumor effect of 2OHOA and its enantiomers, we treated nude mice inoculated with human A549 cells with these compounds over 21 days (Fig. 9). While the RMI enantiomer caused a reduction in tumor volume of about 20–25% after 21 days of treatment (400 mg/kg/day), the SMI enantiomer and the racemic compound caused a reduction of ca. 75%. These results suggest that the presence of 2OHOA in membranes causes about one third of its total anti-tumor effect, and that increase of SM levels would be responsible for approximately two thirds of its anti-cancer effects in this type of cancer.

4. Discussion

The interaction of free FA with membranes occurs in a rapid manner. For instance, it is observed that externally added OA in phosphatidylcholine (PC) giant unilamellar vesicle solutions induce increase in vesicle size after 3 min [29]. It has also been described a destabilization of
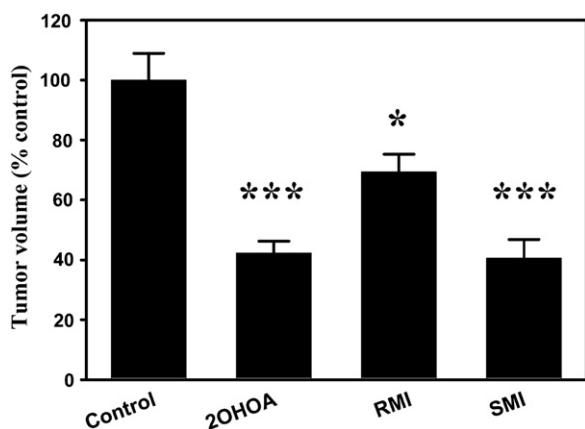
Fig. 9. Anti-tumor efficacy of 2OHOA. Nude mice bearing human lung cancer cell (A549)-derived tumors (subcutaneous xenograft model) were treated orally with the vehicle alone (control), or 400 mg/kg daily for 21 days of 2OHOA or its R and S enantiomers. The bars correspond to the mean ± s.e.m. (relative to the controls) of the tumor volumes at the end of the treatment (n = 12).

giant unilamellar vesicles composed of POPC:PE:SM:CHO (equimolar ratio) after 3-min incubation with different natural and 2-hydroxylated FAs [26]. All in all, the rapid insertion of free FA into membranes and their incorporation in more complex molecules such as phospholipids or triacylglycerides enable these acyl chains to induce changes in the structure of lipid bilayers.

Despite their chemical simplicity, modest modifications in FA structure (e.g., the steric configuration of a double bond) may produce relevant effects in model lipid membranes. However, the molecular requirements to control the lipid structure are different to those to control the activity of proteins, as would be expected given that the molecular entities that form membranes and proteins have distinct types of mobility. Thus, FAs that regulate SGMS activity have one to three double bonds that are configured in cis, a hydroxyl group on C2 and a length of 16–18 carbon atoms. In this context, 2OHOA induces augments of both SGMS1 and SGMS2 activities, whereas it has no effect on SGMS mRNA and protein levels. Interestingly, activation of SGMS by 2OHOA turned out to be extremely rapid and sustained, suggesting a direct interaction between 2OHOA and SGMS. This interaction, which could explain SGMS activation [6,27], would be different for the R and S enantiomers of 2OHOA. In agreement with this, here it is shown that only the S enantiomer of 2OHOA (as well as the S enantiomers of hydroxyl-palmitoleic acid, hydroxy-linoleic and hydroxyl-linolenic acids, results not shown) increases SM levels.

Other FAs that regulate membrane lipid structure also have cis-unsaturations but their effects differ from the aforementioned regulation of SGMS activity in a number of ways. First, although the most relevant membrane regulatory effects are exerted by cis-monounsaturated FAs, FAs with more than 3 double bonds also produce important effects on membrane lipid structure [30,31]. By contrast, we show here that the R or S forms of 2OHOA do not display relevant differences in their effect on membranes. This is an important factor to be considered when designing drugs whose prime target is the lipid bilayer or a peptide. Thus, it would be interesting to know if not only OH radicals but also other types of radicals that can be added to the alpha carbon of fatty acids (e.g., methyl and amino,) might regulate membrane structure and SM content.

All FAs are readily incorporated into all membranes due to their small and comparable molecular volume (ranging from 300 $Å^3$ for EA to 306 $Å^3$ for 2OHOA). Nevertheless, the chemico-physical properties of each FA and of the bilayers used here gives rise to a large variety of interactions. Thus, the addition of 2OHOA to fluid (L_d) membranes leads to an increase in the thickness of the bilayer, whereas in L_o membranes caused a bilayer thinning. This is the result of the interaction

of the hydroxyl groups that increase the surface area of the highly ordered SM:CHO membranes, provoking their thinning. By contrast, the presence of 2OHOA in membranes containing POPC does not alter the lateral packing considerably, although it is responsible for a misfit of the lipid headgroups and a higher membrane curvature [24,25]. These results highlight the contrasting effects on bilayer thickness of ordered and disordered membranes and they are consistent with previous studies showing that 2OHOA also has opposite effects on the organization of ordered and disordered membrane microdomains [27]. In addition, 2OHOA induces a negative bilayer curvature, the R and S enantiomers displaying no significant differences in these terms. By contrast, other FAs do not significantly alter the thickness of the 4 membranes examined in the present study. The promotion of non-lamellar phases induced here by natural and synthetic monounsaturated FAs, as witnessed by molecular dynamics, has been confirmed elsewhere using X-ray scattering, differential scanning calorimetry, NMR, FTIR, etc. [25,26,30,31]. However, the effects of 2OHOA enantiomers are shown here for the first time, and the parallels between molecular modeling and biophysical studies offer support to the results presented here for RMI and SMI.

The presence of FAs in liquid lamellar structures does not significantly alter the potential energy of other lipids. This result confirms the idea that more fluid membranes can easily adapt to external molecules. The insertion of OA and SA into more rigid membranes destabilizes the surrounding lipids in a symmetrical manner and moreover, the presence of FAs in membranes alters the surface packing and the exposure to the water environment. The RDF analyses for POPC and POPC:POPE bilayers indicate that OA and 2OHOA increase the hydration of POPE and POPC molecules, an opposite effect to that of SA, while EA does not perturb the water shell. In lipid raft-like membrane models, SA, EA and 2OHOA increase the hydration of SM molecules, and no differences are observed between RMI and SMI. The complex relationship of surface roughness (and in some cases the surface curvature), lateral packing and the exposure to water is revealed by analyzing the polarization of water dipoles at the surface of the membrane. All FAs affected the alignment of water molecules at the surface of rigid membranes containing SM and CHO. SA, EA and OA also diminished the water polarization in POPC and POPC:POPE membranes, whereas both forms of 2OHOA induced an increase in polarization. The insertion of linear aliphatic chains was responsible for changing the lateral pressure profile, which is primarily responsible for the folding of membrane proteins. Again, no differences were observed for RMI and SMI 2OHOA enantiomers in reducing the stress in the inner core of all four membranes.

X-ray scattering analysis of the effect of 2OHOA and the enantiomers reveals that the effect of all three compounds in membranes was very similar, supporting the data obtained by molecular modeling, and indicating that RMI and SMI exert similar effects on the membrane's lipid structure. By contrast, their effect on SM content was totally different, and while SMI and the racemic mixture induces the marked increase in cellular levels of SM in human U118 cells, the RMI enantiomer had no such effect. This result shows an important difference between the effects of 2OHOA enantiomers on lipid bilayers and enzyme activity. Such divergence, which could be similar for other therapeutic molecules acting on both membrane lipids and proteins, highlights important differences in the molecular mechanisms governing the interactions of the respective enantiomers. The present results suggest a dual mode of action for 2OHOA. On the one hand, the presence of the compound in membranes, either free or in phospholipids regulates the membrane's lipid structure, the order of membrane lipids, the non-lamellar phase propensity and the balance between raft and non-raft membrane domains (type-1 MLT) [24–27,31]. The increase in the non-lamellar phase propensity is associated with PKCα translocation to the membrane and mild activation, followed by the overexpression of the CDK inhibitors, p21[Cip1] and p27[Kip1], and the ensuing inactivation of CDKs, hypophosphorylation of the retinoblastoma protein and inactivation of E2F-1, a key transcription factor for cell proliferation [7,25]. Through

a second anti-cancer mode of action, 2OHOA induces marked increases in the levels of SM (ca. 500%) and concomitant decreases in PE, changing the membrane lipid composition by regulating the activity of an enzyme (type-2 MLT) [6,7]. This event has been associated with Ras transloca-tion from the cell membrane to the cytosol, which inactivates the MAPK and PI3K/Akt pathways [7]. These molecular alterations are induced only in cancer but not in normal cells, where the levels of the SM produced by SGMS are high and there is little substrate (PC and PE), and accordingly, 2OHOA only induces programmed cell death in cancer cells [7,32,33].

Both molecular mechanisms of action are effective against tumor growth, and the fact that only one of the enantiomers can activate SGMS, SMI, made it possible to investigate the relationship between each of these two independent effects on the membrane and the anti-tumor effects of this synthetic fatty acid. In this context, RMI might be responsible with reductions of ca. 25% in the volume of human lung adenocarcinoma-derived tumors, while both the racemic compound and the S enantiomer induce greater reductions in tumor volume, reaching up to 70–75% (Fig. 9). This result suggests that while the effect mediated by 2OHOA through type-1 MLT mechanism constitutes one third of its therapeutic activity, type-2 MLT activity is responsible for around two thirds of the overall anti-cancer effect exerted by this compound. Indeed, the IC_{50} values of the S enantiomer for the growth inhibition of different cell lines were lower than those of RMI.

5. Conclusions

We have investigated the effect of 2OHOA enantiomers and other FAs on the lipid structure of various types of membranes by molecular modeling. Although the presence and configuration of double bonds influenced the structural effects of the various FAs on the membranes, the steric (R or S) configuration of 2OHOA enantiomers did not provoke important changes in the membrane lipid structure. X-ray diffraction studies confirmed these results. By contrast, only the S enantiomer of this synthetic fatty acid induces an increase in SM levels, thereby induc-ing important change in the PE:SM ratio that caused the "proliferation switch" to be turned off in cancer cells. Both molecular events, regula-tion of membrane structure and of SGMS activity, were associated with the anti-tumor effects of 2OHOA and they are additive effects against tumor growth. The present study also highlights the differences in the interaction of drugs with lipid or protein targets.

Abbreviations

2OHOA	2-hydroxy oleic acid
CHO	cholesterol
EA	elaidic acid
FA	fatty acid
H_{II}	hexagonal phase
L_o	liquid-ordered
L_d	liquid-disordered
L_α	liquid crystalline or fluid phase
L_β	gel phase
MLT	membrane lipid therapy
OA	oleic acid
SA	stearic acid
PC	phosphocholine
PE	phosphoethanolamine
POPC	1-palmitoyl,2-oleoyl-sn-glycero-3-phosphocholine
POPE	1-palmitoyl-2-oleoyl-sn-glycero-3-phosphoethanolamine
RDF	radial distribution function
RMI	R-2OHOA
SAXS	small-angle X-ray spectroscopy
SM	sphingomyelin
SMI	S-2OHOA
SGMS	sphingomyelin synthase
WAXS	wide-angle X-ray spectroscopy

References

[1] W. Dowhan, Molecular basis for membrane phospholipid diversity: why are there so many lipids? Annu. Rev. Biochem. 66 (1997) 199–232.
[2] P.V. Escribá, J.M. González-Ros, F.M. Goñi, P.K. Kinnunen, L. Vigh, L. Sánchez-Magraner, A.M. Fernández, X. Busquets, I. Horvath, G. Barceló-Coblijn, Membranes: a meeting point for lipids, proteins and therapies, J. Cell. Mol. Med. 12 (2008) 829–875.
[3] P.V. Escribá, Membrane–lipid therapy: a new approach in molecular medicine, Trends Mol. Med. 12 (2006) 34–43.
[4] A. Cordomi, J. Prades, J. Frau, O. Vögler, S.S. Funari, J.J. Pérez, P.V. Escribá, F. Barceló, Interactions of fatty acids with phosphatidylethanolamine membranes: X-ray dif-fraction and molecular dynamics studies, J. Lipid Res. 51 (2010) 1113–1124.
[5] J. Cerezo, J. Zúñiga, A. Bastida, A. Requena, J.P. Cerón-Carrasco, Atomistic molecular dynamics simulations of the interactions of oleic and 2-hydroxyoleic acids with phosphatidylcholine bilayers, J. Phys. Chem. B 115 (2011) 11727–11738.
[6] G. Barceló-Coblijn, M.L. Martin, R.F. de Almeida, M.A. Noguera-Salva, A. Marcilla-Etxenike, F. Guardiola-Serrano, A. Luth, B. Kleuser, J.E. Halver, P.V. Escribá, Sphingomyelin and sphingomyelin synthase (SMS) in the malignant transformation of glioma cells and in 2-hydroxyoleic acid therapy, Proc. Natl. Acad. Sci. U. S. A. 108 (2011) 19569–19574.
[7] S. Terés, V. Lladó, M. Higuera, G. Barceló-Coblijn, M.L. Martin, M.A. Noguera-Salvá, A. Marcilla-Etxenike, J.M. Garcia-Verdugo, M. Soriano-Navarro, C. Saus, U. Gomez-Pinedo, X. Busquets, P.V. Escribá, 2-Hydroxyoleate, a nontoxic membrane binding anticancer drug, induces glioma cell differentiation and autophagy, Proc. Natl. Acad. Sci. U. S. A. 109 (2012) 8489–8494.
[8] T. Crul, N. Toth, S. Piotto, P. Literati-Nagy, K. Tory, P. Haldimann, B. Kalmar, L. Greensmith, Z. Torok, G. Balogh, Hydroximic acid derivatives: pleiotropic Hsp co-inducers restoring homeostasis and robustness, Curr. Pharm. Des. 19 (2013) 309–346.
[9] I. Gombos, T. Crul, S. Piotto, B. Gungor, Z. Torok, G. Balogh, M. Peter, J.P. Slotte, F. Campana, A.M. Pilbat, A. Hunya, N. Toth, Z. Literati-Nagy, L. Vigh Jr., A. Glatz, M. Brameshuber, G.J. Schutz, A. Hevener, M.A. Febbraio, I. Horvath, L. Vigh, Membrane–lipid therapy in operation: the HSP co-inducer BGP-15 activates stress signal transduction pathways by remodeling plasma membrane rafts, PLoS One 6 (2011) e28818.
[10] N. Kucerka, S. Tristram-Nagle, J.F. Nagle, Structure of fully hydrated fluid phase lipid bilayers with monounsaturated chains, J. Membr. Biol. 208 (2005) 193–202.
[11] E. Krieger, T. Darden, S. Nabuurs, A. Finkelstein, G. Vriend, Making optimal use of empirical energy functions: force-field parameterization in crystal space, Proteins 57 (2004) 678–683.
[12] H.J.C. Berendsen, J.P.M. Postma, W.F. van Gunsteren, A. Di Nola, J.R. Haak, Molecular dynamics with coupling to an external bath, J. Chem. Phys. 81 (1984) 3684–3698.
[13] Y. Duan, C. Wu, S. Chowdhury, M.C. Lee, G. Xiong, W. Zhang, R. Yang, P. Cieplak, R. Luo, T. Lee, J. Caldwell, J. Wang, P. Kollman, A point-charge force field for molecular mechanics simulations of proteins based on condensed-phase quantum mechanical calculations, J. Comput. Chem. 24 (2003) 1999–2012.
[14] A. Klamt, Conductor-like screening model for real solvents. A new approach to the quantitative calculation of solvatation phenomena, J. Phys. Chem. 99 (1995) 2224–2235.
[15] J.J. Stewart, MOPAC: a semiempirical molecular orbital program, J. Computer-Aided Mol. Des. 4 (1990) 1–105.
[16] U. Essmann, L. Perera, M.L. Berkowitz, T. Darden, H. Lee, L.G. Pedersen, A smooth particle mesh Ewald method, J. Chem. Phys. 103 (1995) 9877–9893.
[17] R.S. Cantor, The influence of membrane lateral pressures on simple geometric models of protein conformational equilibria, Chem. Phys. Lipids 101 (1999) 45–56.
[18] D. Marsh, Lateral pressure in membranes, Biochim. Biophys. Acta 1286 (1996) 183–223.
[19] R.J. Hardy, Formulas for determining local properties in molecular-dynamics simula-tions: shock waves, J. Chem. Phys. 76 (1982) 622–629.
[20] J.J. Stewart, Application of localized molecular orbitals to the solution of semiempir-ical self-consistent field equations, Int. J. Quantum Chem. 58 (1996) 133–146.
[21] J.J.P. Stewart, MOPAC2012, Stewart Computational Chemistry, Colorado Springs, CO., USA, 2012.
[22] E.G. Bligh, W.J. Dyer, A rapid method of total lipid extraction and purification, Can. J. Biochem. Physiol. 37 (1959) 911–917.
[23] G.P. Gellermann, T.R. Appel, A. Tannert, A. Radestock, P. Hortschansky, V. Schroeckh, C. Leisner, T. Lutkepohl, S. Shtrasburg, C. Rocken, M. Pras, R.P. Linke, S. Diekmann, M. Fandrich, Raft lipids as common components of human extracellular amyloid fibrils, Proc. Natl. Acad. Sci. U. S. A. 102 (2005) 6297–6302.

[24] F. Barceló, J. Prades, S.S. Funari, J. Frau, R. Alemany, P.V. Escribá, The hypotensive drug 2-hydroxyoleic acid modifies the structural properties of model membranes, Mol. Membr. Biol. 21 (2004) 261–268.

[25] J. Martínez, O. Vögler, J. Casas, F. Barcelo, R. Alemany, J. Prades, T. Nagy, C. Baamonde, P.G. Kasprzyk, S. Terés, C. Saus, P.V. Escribá, Membrane structure modulation, protein kinase C alpha activation, and anticancer activity of minerval, Mol. Pharmacol. 67 (2005) 531–540.

[26] M. Ibarguren, D.J. López, J.A. Encinar, J.M. González-Ros, X. Busquets, P.V. Escribá, Partitioning of liquid-ordered/liquid-disordered membrane microdomains induced by the fluidifying effect of 2-hydroxylated fatty acid derivatives, Biochim. Biophys. Acta 1828 (2013) 2553–2563.

[27] M.L. Martin, G. Barceló-Coblijn, R.F. de Almeida, M.A. Noguera-Salva, S. Terés, M. Higuera, G. Liebisch, G. Schmitz, X. Busquets, P.V. Escribá, The role of membrane fatty acid remodeling in the antitumor mechanism of action of 2-hydroxyoleic acid, Biochim. Biophys. Acta 1828 (2013) 1405–1413.

[28] V. Lladó, S. Terés, M. Higuera, R. Álvarez, M.A. Noguera-Salva, J.E. Halver, P.V. Escribá, X. Busquets, Pivotal role of dihydrofolate reductase knockdown in the

[29] anticancer activity of 2-hydroxyoleic acid, Proc. Natl. Acad. Sci. U. S. A. 106 (2009) 13754–13758.

[29] M. Mally, P. Peterlin, S. Svetina, Partitioning of oleic acid into phosphatidylcholine membranes is amplified by strain, J. Phys. Chem. B 117 (2013) 12086–12094.

[30] R.M. Epand, R.F. Epand, N. Ahmed, R. Chen, Promotion of hexagonal phase formation and lipid mixing by fatty acids with varying degrees of unsaturation, Chem. Phys. Lipids 57 (1991) 75–80.

[31] S. Piotto, A. Trapani, E. Bianchino, M. Ibarguren, D.J. Lopez, X. Busquets, S. Concilio, The effect of hydroxylated fatty acid-containing phospholipids in the remodeling of lipid membranes, Biochim. Biophys. Acta Biomembr. (2014)(in this issue).

[32] V. Lladó, S. Terés, M. Higuera, R. Álvarez, M.A. Noguera-Salva, J.E. Halver, P.V. Escribá, X. Busquets, Pivotal role of dihydrofolate reductase knockdown in the anticancer activity of 2-hydroxyoleic acid, Proc. Natl. Acad. Sci. 106 (2009) 13754–13758.

[33] S. Terés, V. Lladó, M. Higuera, G. Barceló-Coblijn, M.L. Martin, M.A. Noguera-Salvà, A. Marcilla-Etxenike, J.M. García-Verdugo, M. Soriano-Navarro, C. Saus, Normalization of sphingomyelin levels by 2-hydroxyoleic acid induces autophagic cell death of SF767 cancer cells, Autophagy 8 (2012) 1542–1544.